International Journal of Remote Sensing
Vol. 26, No. 18, 20 September 2005, 3985–4000

Taylor & Francis
Taylor & Francis Group

In situ surface temperature retrieval in a boreal forest under variable cloudiness conditions

R. NICLÒS*, V. CASELLES, C. COLL, E. VALOR and J. M. SÁNCHEZ
Department of Thermodynamics, Faculty of Physics, University of Valencia, 50 Dr. Moliner, 46100 Burjassot, Valencia, Spain

(*Received 8 June 2004; in final form 3 May 2005*)

Canopy temperature retrieval was one of the purposes during the Solar Induced FLuorescence EXperiment (SIFLEX-2002) of the European Space Agency, carried out in a Finnish boreal forest. In this work, we describe the strategy used to determine this temperature from ground thermal infrared (TIR) data under skies with variable cloud cover. TIR radiance was measured by a CIMEL Electronique CE 312 radiometer. An analysis of the radiative transfer equation showed which terms were necessary to obtain accurate surface temperatures during the campaign. Atmospheric correction was considered negligible due to the small atmospheric path, but hemispheric downwelling sky radiance determination was needed for the emissivity correction. Since most days during the campaign the sky showed partial cloudiness, a methodology to estimate this last term was proposed, using continuous information of cloudiness amount and cloud height given by a weather station. These thermal data were used to analyse some correlations between canopy and air temperatures and plant-activity-related variables in the context of the SIFLEX-2002 campaign.

1. Introduction

The present study was developed in the framework of the European Space Agency's project Solar Induced FLuorescence EXperiment (SIFLEX-2002). Its main objective was to collect experimental data to investigate the impact of the change in photosynthetic activity of a boreal forest on remote sensing observables, such as chlorophyll fluorescence and physiological reflectance index (PRI). This experiment represented a significant step towards the improvement of the development of fluorescence models, with the future aim of using these measurements to map the activity of vegetation masses from space and to analyse their fluctuations and impact. The field campaign was carried out from April to June 2002 in a boreal forest region of northern Finland, covering the spring recovery of the forest from winter dormancy to its fully active summer state when photosynthesis was at a maximum.

Our purpose in this experiment was to determine accurately air and surface temperatures in order to characterize their circadian cycle and fluctuations in this natural environment over the whole duration of the campaign. These thermal data were required to analyse possible correlations between their temporal variation and that of measurements on the same target of variables related to plant functioning,

*Corresponding author. Email: Raquel.Niclos@uv.es

International Journal of Remote Sensing
ISSN 0143-1161 print/ISSN 1366-5901 online
http://www.tandf.co.uk/journals
DOI: 10.1080/01431160500180954

such as fluorescence signal and PRI. Air temperature (T_a) was measured in the target with a thermocouple. The surface temperature (T_c) was measured using a high-resolution and thermal infrared (TIR) multichannel radiometer with an adequate radiometric resolution to detect small surface–air temperature differences. This paper presents the measurement strategy and the data corrections used to retrieve canopy temperature from TIR measurements, in which the effect of the downwelling sky radiation is the most important issue. A methodology has been developed to determine sky radiation under partial cloud cover conditions, which was the most usual situation during the campaign.

In the next section a description of the experimental site and the instrumentation is given. Section 3 presents in detail the proposed methodology for retrieving surface temperature, with special consideration to the measurement of the downwelling sky irradiation. In section 4 a sensitivity analysis is included, and section 5 shows the temperatures obtained by the methodology for the boreal forest. Moreover, the first results about the relationships between air and canopy temperatures, the PRI and other meteorological variables are pointed out. Finally, the main conclusions are given in section 6.

2. Experimental site, instrumentation and measurement strategy

The experimental site was a Finnish boreal forest region placed at 67°21′42.7″ N and 26°38′16.2″ E, 179 m above sea level and 100 km north of the Arctic Circle (figure 1(*a*)). This experimental area belongs to the Arctic Research Centre of the Finnish Meteorological Institute (FMI), at Sodankylä, which is a reference site for studies about carbon dioxide fluxes. Vegetation in this area is composed of Scots pines (*Pinus sylvestris* L.) more than 10 m in height and an average age of 100 years. The tree density is 2100 trunks ha^{-1}, with a leaf area index (LAI) of 1.2, and the soil is fluvial sandy podzol.

During the SIFLEX campaign the following data were collected: (i) boreal forest photosynthetic activity variables, such as fluorescence signal, PRI and photosynthetically active radiance (PAR) measurements, by the Laboratoire pour l'Utilisation du Rayonnement Electromagnétique (LURE, Orsay, France), using two passive fluorimeters, a self-constructed BiDetector (BD; Moya *et al.* 2002), operating solely in the atmospheric oxygen A band, a passive multi-wavelength fluorescence detector (PMFD) (Evain *et al.* 2001) and two active frequency-induced PAM fluorimeters (FIPAM) (Flexas *et al.* 2000); (ii) global, direct and diffuse radiation, using Li-Cor 1800 spectroradiometers (Cachorro *et al.* 1997), surface radiance with a CIMEL Electronique CE 312 thermal radiometer (Legrand *et al.* 2000), and three-dimensional canopy reconstruction by means of stereovision cameras, all measured by the University of Valencia (Spain); and (iii) meteorological parameters, cloud cover and height, atmospheric radiosounding profiles, carbon dioxide flux, and sensible and latent heat fluxes with a SATI-3Sx sonic anemometer and a platinum thermal probe by using eddy-covariance methodology (Aurela *et al.* 2001), obtained by the FMI.

Thermal data acquisition over the tops of the pine trees (see the target in figure 1(*b*)) was our purpose during this campaign. Air temperature (T_a) measurements were carried out by a type K thermocouple every 10 minutes. This was located at the height of the tree tops inside the target area and protected from rain and direct radiation by an open box. Before the measurements, this thermocouple was calibrated within the air temperature range expected during the

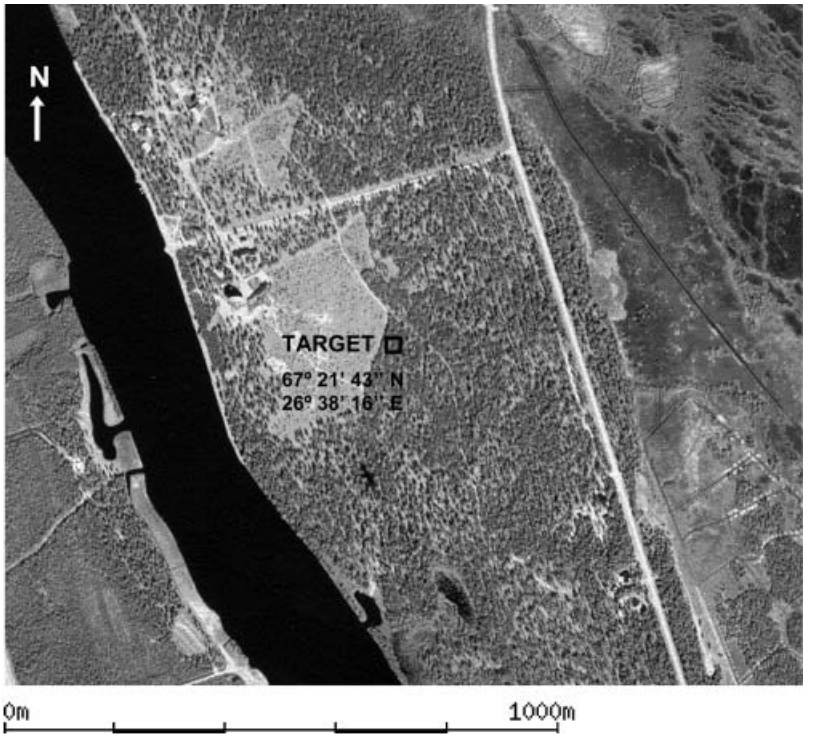

(*a*)

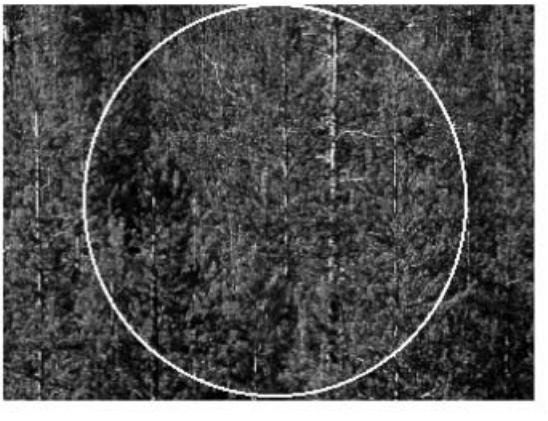

(*b*)

Figure 1. (*a*) Aerial photograph of the region belonging to the Arctic Research Centre, where the experimental site of the SIFLEX-2002 project is marked by a square. (*b*) CE 312 radiometer view of the canopy target during the campaign.

campaign, from about 265 K to 303 K, by means of stirred liquid baths using a 1/10 DIN Pt-100 probe as a reference. After calibration, T_a accuracy was better than ± 0.1 K.

Canopy (branches and leaves of Scots pine trees) thermal radiance measurements were performed autonomously every 10 minutes by the CE 312 TIR radiometer,

which has four spectral channels: one broadband, 8–14 μm (band 1), and three narrow channels, 11.5–12.5 μm, 10.5–11.5 μm and 8.2–9.2 μm (bands 2, 3 and 4, respectively) (Legrand *et al.* 2000). Figure 2 shows the normalized spectral response functions of the CE 312 channels, together with the atmospheric transmittance corresponding to the sub-Arctic summer and winter standard atmospheric profiles in order to show the relative transparency of the narrow channels. The radiometer has a field of view of 10°, a response time of 1 second, and a radiometric temperature resolution of ±8 mK for the broadband and ±50 mK for the other channels, which is adequate for detecting small differences between canopy and air temperatures. The brightness temperature accuracies are ±0.10 K, ±0.12 K, ±0.09 K and ±0.14 K for channels 1–4, respectively, which have been evaluated from a large number of calibration processes of the radiometer carried out under a wide range of thermal conditions. The temperature of the cavity containing the detector, which is measured by a Pt-100 probe attached to the detector surface, is used as a temperature reference. The radiometer is also provided with a concealable, gold-coated mirror, which allows comparisons between the radiance coming from an external target and the reference radiation from inside the optical head cavity to correct measurements from the radiometer's cavity self-radiation, taking into account possible variations in the head temperature.

During the SIFLEX campaign, the radiometer observed the vegetation target over which the fluorescence signal and PRI were measured simultaneously. The radiometer was placed at a height of 12 m from the ground, 4 m above the tree tops. The observation angle was fixed at 85° from nadir, using a quasi-horizontal path to assure a homogeneous view of the vegetation (see figure 1(*b*)), and to avoid the observation of the soil, which had a variable snow cover during the campaign. Thus,

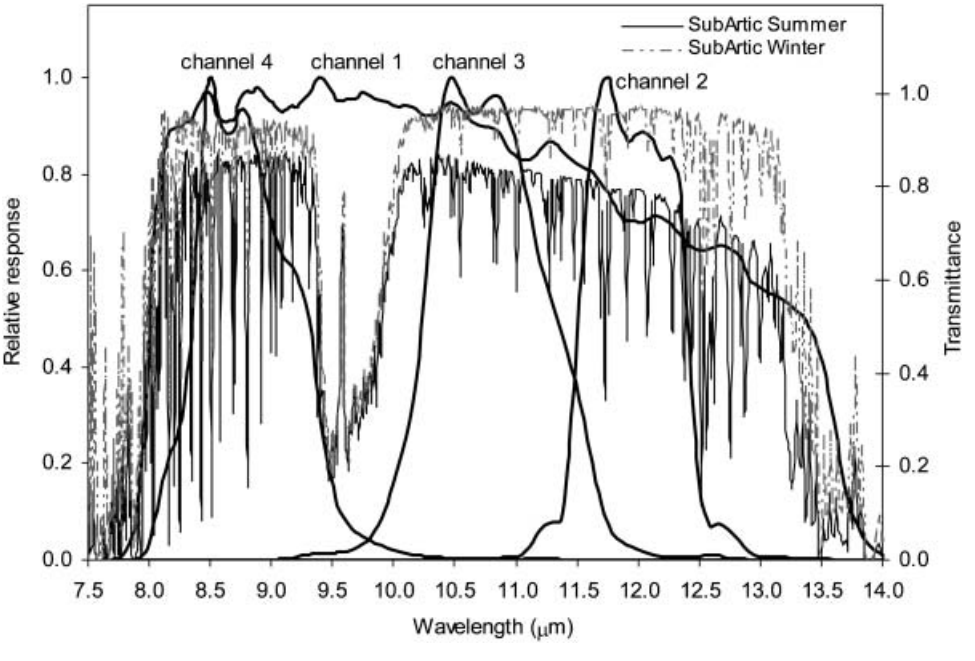

Figure 2. Spectral response functions of the CE 312 radiometer channels. Atmospheric transmittances for the sub-Arctic summer and winter standard atmospheric profiles are shown on the secondary axis.

a quasi-horizontal path of 46 m in length was considered, and the target area (within the white circle of figure 1(*b*)) was of about 42 m^2. In addition, we checked the effect of possible pointing errors by changing the observation angle slightly, and the thermal spatial variability around the target was negligible.

The radiometer was kept in a shelter to be protected from adverse environmental conditions and the incoming radiance was observed through a ZnSe window 4 mm thick, which was selected because of its good transmission within the TIR region. Moreover, a small bag of silica gel was placed inside the protective shelter to prevent condensation. For this reason, a calibration of the radiometer viewing through the protective window was carried out in the field conditions to cover the observed temperature range (from 265 K to about 303 K), where the optical properties of the window were taken into account. A black-body calibration source was used as reference for that purpose and its temperature was measured using an internal Pt-100 probe. A calibration function was obtained for each channel:

$$R_{m,i} = \tau_i B_i(T_s) + \rho_i B_i(T_{int}) + \alpha_i B_i(T_w) \quad (1)$$

where $R_{m,i}$ is the CE 312 radiance measured through the ZnSe window in channel i; $B_i(T)$ is the channel i averaged Planck's function for a temperature T; T_s is the source temperature; T_{int} is the internal temperature of the radiometer's optical head measured by the Pt-100 probe placed inside the optical head, which has an uncertainty of ± 0.1 K; T_w is the ZnSe window temperature; and α_i, ρ_i and τ_i are the window absorptance, reflectance and transmittance, respectively. Equation (1) can be rewritten, through $\alpha_i + \rho_i + \tau_i = 1$, as follows:

$$R_{m,i} - B_i(T_{int}) = \tau_i(B_i(T_s) - B_i(T_{int})) + \zeta_i \quad (2)$$

with $\zeta_i = \alpha_i(B_i(T_w) - B_i(T_{int}))$. Since T_{int} and T_w could be considered similar and correlated, because it is reasonable to assume that they would be similarly affected by air temperature variations during the day, ζ_i was practically a constant. Thus, a linear regression of $R_{m,i} - B_i(T_{int})$ on $B_i(T_s) - B_i(T_{int})$ allowed the determination of the calibration parameters τ_i and ζ_i. The calibration coefficients are presented in table 1, in which their variability, given by the standard deviation, allows a check on the instrument's stability and the minimum contamination effect of the ZnSe window during the campaign.

$B_i(T_s)$ can be determined from equation (2), from which the calibrated brightness temperature, T_s, is obtained. The uncertainty of T_s was estimated by applying the error theory to the defined calibration equation and using the CE 312 data measured

Table 1. Calibration coefficients, τ_i and ζ_i (equation (2)), obtained for the CE 312 channels in SIFLEX-2002 campaign. Standard deviations of the coefficients, σ, and determination coefficients of the regressions, r_i^2, are also indicated. $\sigma(T_{s,i})$ is the average uncetainty of canopy brightness temperature after the calibration process.

Channel	τ_i	$\pm\sigma(\tau_i)$	ζ_i^*	$\pm\sigma(\zeta_i)^*$	r_i^2	$\pm\sigma(T_{s,i})$ (*K*)
1 (8–14 μm)	0.7510	0.0013	0.3	1.2	0.999	0.15
2 (11.5–12.5 μm)	0.7439	0.0017	− 9.0	1.7	0.999	0.19
3 (10.5–11.5 μm)	0.7561	0.0019	− 6.9	1.8	0.999	0.13
4 (8.2–9.2 μm)	0.771	0.003	− 5.8	2.1	0.998	0.2

*In 10^{-6} mW $(cm^2\,sr\,cm^{-1})^{-1}$.

during the SIFLEX campaign. Finally, canopy brightness temperature uncertainties of ± 0.15 K, ± 0.19 K, ± 0.13 K and ± 0.2 K were obtained for the CE 312 channels 1 to 4, respectively (table 1). Channel 3 (10.5–11.5 μm) shows the highest precision after the calibration process.

3. Methodology

The radiance reaching the CE 312 radiometer, separated by a distance h from the target and measured by channel i under an observation angle θ, $R_i(\theta, h)$, is composed of two main contributions: (i) the radiance at target level, which involves the canopy direct emission and the reflection of the hemispheric downwelling sky radiance on the canopy, both attenuated by the absorption of the atmosphere between the target and the instrument, characterized by the path transmittance, $\tau_i(\theta, 0, h)$; and (ii) the path radiance emitted by the atmosphere in the viewing direction, $L^{\uparrow}_{i\ atm}(\theta)$, as follows:

$$R_i(\theta, h) = \left\{ \varepsilon_i(\theta) B_i(T_c) + [1 - \varepsilon_i(\theta)] L^{\downarrow}_{i\ atm\ hem} \right\} \tau_i(\theta, 0, h) + L^{\uparrow}_{i\ atm}(\theta) \tag{3}$$

where $B_i(T_c)$ is the channel i averaged Planck's function for a canopy temperature, T_c; $\varepsilon_i(\theta)$ is the emissivity; and $L^{\downarrow}_{i\ atm\ hem}$ is the hemispheric downwelling sky radiance, i.e. the effective sky radiance corresponding to the downward emission of the whole atmosphere.

Canopy temperature can be written as:

$$T_c = T_i + \Delta T_{i,\ atm} + \Delta T_{i,\ \varepsilon} \tag{4}$$

where T_i is the measured brightness temperature, obtained under the assumption $R_i(\theta, h) = B_i(T_i)$, and $\Delta T_{i,\varepsilon}$ and $\Delta T_{i,atm}$ represent the emissivity and atmospheric path corrections in terms of temperature.

The atmospheric path correction can be considered negligible due to the short radiometer-to-target distance used during this campaign, mainly for channel 3 (10.5–11.5 μm), for which a $\Delta T_{i,atm}$ of 0.03 K was estimated using $\tau_i(\theta, 0, h)$ and $L^{\uparrow}_{i\ atm}(\theta)$ values simulated with the MODTRAN 4 radiative transfer code (Berk *et al.* 1999) and radiosounding data launched in the experimental site, in front of the 0.12 K obtained for channel 1 (8–14 μm). The $\Delta T_{i,atm}$ difference between the two channels proves the soundness of radiometers measuring within the 10.5–11.5 μm region instead of most field radiometers that work in the 8–14 μm broadband. CE 312 channel 3 also showed the lowest measurement dispersion. Consequently, the spectral band 10.5–11.5 μm was used for the T_c retrieval in this work, and the approximations $\tau_i(\theta, 0, h) \approx 1$ and $L^{\uparrow}_{i\ atm}(\theta) \approx 0$ were considered in equation (3). However, the surface emissivity and the hemispheric downwelling sky radiance, i.e. the emissivity correction, are still necessary for T_c retrieval.

3.1 *Emissivity correction*

Emissivity correction is determined in terms of temperature as $\Delta T_{i,\varepsilon} = T_c - T_i$, which can be obtained from equation (3) as follows:

$$\Delta T_{i,\ \varepsilon} = \left\{ \left[\frac{1 - \varepsilon_i(\theta)}{\varepsilon_i(\theta)} \right] \left[R_i(\theta, h) - L^{\downarrow}_{i\ atm\ hem} \right] \right\} \left[\frac{\partial B_i(T)}{\partial T} \right]^{-1} \tag{5}$$

The surface emissivity, $\varepsilon_i(\theta)$, is probably the parameter that needs the most accurate determination due to its important effect in T_c retrieval. In order to determine the emissivity of the target (i.e. the vertical side of the pine tops), pine branches were collected and disposed horizontally in homogeneous layers. This target emissivity was measured at nadir using the Box Method (Rubio *et al.* 1997, 2003) with the CE 312 radiometer, obtaining values of 0.978 ± 0.003, 0.975 ± 0.003, 0.973 ± 0.002 and 0.975 ± 0.003 for channels 1 to 4, respectively.

To calculate $L^{\downarrow}_{i\ atm\ hem}$, atmospheric profiles representative of the whole atmosphere are needed. Sub-Arctic winter and summer standard atmospheres were used. Some of the radiosoundings launched in the region during the campaign were also selected as a reference since they were representative of two extreme sky conditions: completely clear and completely cloudy days (0 octas, and 8 octas of stratocumulus with a base height of 300 m, respectively). All of them were introduced into the MODTRAN 4 code in order to calculate the corresponding $L^{\downarrow}_{i\ atm\ hem}$ contribution for those situations for which an atmospheric effective angle was used (see section 3.2). Emissivity correction was determined with equation (5) for all of them. Table 2 shows as an example average values of the emissivity correction applied to each atmospheric profile, $\Delta T_{i,\varepsilon}$, for a completely clear sky and for a completely cloudy sky with three different kinds of clouds, characterized by the cloud base height, H. In addition, the effect of the downwelling sky radiance on the emissivity correction can be estimated separately to check its importance in each case. The values of the emissivity correction if the downwelling sky radiance was neglected, $\Delta T_{i,\varepsilon}'$, are shown. The last row presents the contribution to the emissivity correction due to $L^{\downarrow}_{i\ atm\ hem}$ alone, which is obtained by simply subtracting $\Delta T_{i,\varepsilon}'$ from $\Delta T_{i,\varepsilon}$.

For sub-Arctic completely clear skies, the lowest impact of $L^{\downarrow}_{i\ atm\ hem}$ in terms of temperature is observed in channel 3 again (-0.13 K), and it seems negligible. On the contrary, under cloudy skies with low clouds, a T_c decrease up to 1.5 K would be possible if the $L^{\downarrow}_{i\ atm\ hem}$ term were not considered. Therefore, the hemispheric downwelling sky radiance is needed to obtain accurate T_c measurements.

Table 2. Emissivity correction, $\Delta T_{i,\varepsilon}$(K); emissivity correction without the downwelling sky radiance contribution, $\Delta T_{i,\varepsilon}'$(K); and effect of the downwelling sky radiance in terms of temperature, $\Delta T_{i,\varepsilon} - \Delta T_{i,\varepsilon}'$(K). All these terms are provided for the CE 312 channels and different cloudiness conditions (no clouds, and completely covered skies with different kinds of clouds: altostratus, cumulus and nimbostratus).

		Channel 1 (8–14 μm)	Channel 2 (11.5–12.5 μm)	Channel 3 (10.5–11.5 μm)	Channel 4 (8.2–9.2 μm)
$\Delta T_{i,\varepsilon}$(K)	No clouds	1.02	1.43	1.47	1.03
	Altostratus (H=2.5 km)	0.28	0.32	0.35	0.32
	Cumulus (H=0.66 km)	0.17	0.20	0.21	0.20
	Nimbostratus (H=0.16 km)	0.14	0.16	0.17	0.17
$\Delta T_{i,\varepsilon}'$(K)		1.25	1.68	1.60	1.24
$\Delta T_{i,\varepsilon} - \Delta T_{i,\varepsilon}'$(K)	No clouds	− 0.23	− 0.25	− 0.13	− 0.21
	Altostratus (H=2.5 km)	− 0.97	− 1.36	− 1.25	− 0.91
	Cumulus (H=0.66 km)	− 1.08	− 1.48	− 1.39	− 1.04
	Nimbostratus (H=0.16 km)	− 1.11	− 1.51	− 1.43	− 1.07

3.2 *Determination of hemispheric downwelling sky radiance*

The hemispheric downwelling sky radiance, $L^{\downarrow}_{i\ atm\ hem}$, is given as an integration of the radiance emitted downwards in every direction, defined by θ and ϕ, $L^{\downarrow}_{i\ atm}(\theta, \phi)$, and divided by π. Thus, to measure this hemispheric downwelling sky radiance involves performing a scanning of the atmospheric radiance varying the zenith and azimuth angles of observation, using a goniometric system of pointing. This process is very lengthy, and the retrieved $L^{\downarrow}_{i\ atm\ hem}$ cannot be simultaneous to the canopy radiance measurement due to the long time required (each directional measurement takes 1.2 minutes approximately), even using a second radiometer. To avoid this long scanning process, there are approximate methods for estimating $L^{\downarrow}_{i\ atm\ \ hem}$ from a single direction radiance measurement, all of them under conditions of horizontal homogeneity of the atmosphere, i.e. for completely cloud-free or cloudy skies (Rubio *et al.* 1997).

For example, we can use the approximation $L^{\downarrow}_{i\ atm\ \ hem} \approx L^{\downarrow}_{i\ atm}(\theta_{ef,i})$ (Kondratyev 1969), where $\theta_{ef,i}$ is considered as an effective angle of about 53° that varies slightly with the atmospheric conditions and the measurement spectral band thought a parameter x_i. The effective angle can be retrieved as:

$$\theta_{ef,i} \approx \arccos\left[\left(\frac{2-x_i}{2}\right)^{1/x_i}\right] \tag{6}$$

where the term $(2 - x_i)/2$ is the ratio between the $L^{\downarrow}_{i\ atm\ hem}$ and the downwelling sky radiance measured at zenith, $L^{\downarrow}_{i\ atm}(0^{\circ})$.

A study of the angular variation of the downwelling sky radiance has been carried out in this work. Here, sub-Arctic summer and winter atmospheres under completely clear and cloudy sky conditions, with different kinds of clouds, were considered. Downwelling sky radiance for several zenith angles from 0° to 85° for these atmospheric profiles has been simulated using MODTRAN 4. Table 3 shows the atmospheric effective angle, $\theta_{ef,i}$, for winter and summer sub-Arctic atmospheres under completely clear sky conditions. The effective angle is lower for summer than for winter, showing an additional dependence on the spectral channel. Moreover, the ratio $(2 - x_i)/2$ is about 1.4 for the sub-Arctic profiles and no-cloud conditions but it is equal to unity for cloudy skies, mainly for low clouds, which is obviously due to the low angular dependence shown by $L^{\downarrow}_{i\ atm}(\theta)$ under these conditions. Thus, $\theta_{ef,i}$ calculated for cloudy skies, with a value of approximately 53° both for summer and winter, is not significant because the negligible angular dependence drives to obtain practically the same radiance for any view angle, i.e. downwelling radiance is quasi-isotropic, and the hemispheric radiance could be measured directly at zenith. However, the $L^{\downarrow}_{i\ atm}(\theta)$ angular variation is strong for clear skies but the effect of the downwelling sky radiance on T_c retrieval is small for cloud-free sub-Arctic atmospheres (-0.13 K for channel 3; see table 2).

Table 3. Effective angle, $\theta_{ef,i}$, calculated for summer and winter sub-Arctic atmospheres under completely clear skies.

$\theta_{ef,i}$(deg)	Channel 1 (8–14 μm)	Channel 2 (11.5–12.5 μm)	Channel 3 (10.5–11.5 μm)	Channel 4 (8.2–9.2 μm)
Summer	55.55 ± 0.10	55.54 ± 0.14	56.80 ± 0.12	55.83 ± 0.08
Winter	56.06 ± 0.04	57.76 ± 0.06	58.29 ± 0.04	56.60 ± 0.04

There was, however, hardly ever horizontal homogeneity of the atmosphere during the campaign, but partial cloud cover, and the above approximations were not valid for these sky conditions. Thus, a strategy was developed to account for the $L^{\downarrow}_{i\ atm\ hem}$ term in these conditions of partial cover.

The main contribution to $L^{\downarrow}_{i\ atm\ hem}$ is due to the cloudiness amount, measured as number of octas, and cloud base height, H, which determines its temperature. Representative radiosoundings performed under completely cloudy skies for different cloudiness height were introduced into the MODTRAN 4 code in order to obtain the hemispheric downwelling sky radiance emitted by clouds, $L^{\downarrow}_{i\ atm\ hem,C}$, as a function of their height, H. Additionally, $L^{\downarrow}_{i\ atm\ hem,C}$ simulations using the cloud extensions of MODTRAN 4 on the sub-Arctic standard profiles for summer and winter were used, distinguishing among: nimbostratus (H=0.16 km), stratus (H=0.33 km), stratocumulus and cumulus (H=0.66 km) and altostratus (H=2.4 km). Linear regressions between $L^{\downarrow}_{i\ atm\ hem,C}$ and H were determined for cloud downward emission as:

$$L^{\downarrow}_{i\ atm\ hem,C} = m_i H + n_i \tag{7}$$

showing differences for summer and winter conditions. Table 4 shows the regression coefficients of equation (7), m_i and n_i, their standard deviations, $\sigma(m_i)$ and $\sigma(n_i)$, and the determination coefficients of these regressions, r_i^2.

The variability in cloudiness conditions was determined using the Sodankylä weather database, given by the Finnish Meteorological Institute (FMI), where number of octas, C, from 0 to 8, and cloud base height measured by a Vaisala ceilometer (Lonnqvist 1995), H, were available in an almost continuous way. Finally, the following approximation was considered to obtain $L^{\downarrow}_{i\ atm\ hem}$:

$$L^{\downarrow}_{i\ atm\ hem} = \left(\frac{C}{8}\right) L^{\downarrow}_{i\ atm\ hem,C} + \left(1 - \frac{C}{8}\right) L^{\downarrow}_{i\ atm\ hem,NC} \tag{8}$$

where $L^{\downarrow}_{i\ atm\ hem,NC}$ is the downwelling sky radiance for the completely clear sky. This term was simulated by means of the MODTRAN 4 code for sub-Arctic standard atmospheres at the observation angles $\theta_{ef,i}$ provided in table 3, and checked with direct CE 312 measurements four times a day. The contribution of clouds to the downwelling sky radiance, $L^{\downarrow}_{i\ atm\ hem,C}$, was determined by applying equation (8), with the coefficients shown in table 4, to each instantaneous H value.

This approximation represents a useful method to retrieve the hemispheric downwelling sky radiance under partial cloud cover, taking into account that for the cloudy parts the sky radiance angular variation is negligible, and for the clear parts the impact of the angular dependence is low due to the low sky radiance of sub-Arctic atmospheres, as has been shown in table 2.

4. Sensitivity analysis

Since the atmospheric correction is negligible (i.e. $\tau_i(0, h) \approx 1$ and $L^{\uparrow}_{i\ atm} \approx 0$), T_c can be computed from surface radiance and hemispheric downwelling sky radiance directly using equation (3). The T_c uncertainty, $\sigma(T_c)$, can be derived from this equation by applying error theory as:

$$\sigma(T_c) = \left|\frac{\partial T_c}{\partial B_i(T_c)}\right| \sigma(B_i(T_c)) \tag{9}$$

Table 4. Regression coefficients of equation (7): slope, m_i, constant, n_i, their standard deviations, $\sigma(m_i)$ and $\sigma(n_i)$, standard error of estimate, $\sigma'(L^{\downarrow}_{i\ atm\ hem,C})$, and the determination coefficients of the regressions, r_i^2, for the CE 312 channels.

Atmosphere	Channel	m_i^*	$\pm\sigma(m_i)^*$	$n_i^\dagger$	$\pm\sigma(n_i)^\dagger$	$\sigma'(L^{\downarrow}_{i\ atm\ hem,C})^\dagger$	r_i^2
Sub-Arctic summer	1 (8–14 μm)	− 4.83	0.10	7.783	0.011	0.017	0.999
	2 (11.5–12.5 μm)	− 5.42	0.14	10.576	0.016	0.02	0.998
	3 (10.5–11.5 μm)	− 5.86	0.10	9.047	0.012	0.018	0.999
	4 (8.2–9.2 μm)	− 4.2	0.2	5.74	0.03	0.04	0.992
Sub-Arctic winter	1 (8–14 μm)	− 1.4	0.3	4.65	0.04	0.06	0.880
	2 (11.5–12.5 μm)	− 1.8	0.4	6.75	0.05	0.08	0.844
	3 (10.5–11.5 μm)	− 1.7	0.4	5.51	0.05	0.07	0.869
	4 (8.2–9.2 μm)	− 1.2	0.2	3.15	0.03	0.04	0.890

*In 10^{-4} (mW (cm^2 sr cm^{-1})$^{-1}$) km^{-1}.
†In 10^{-3} mW (cm^2 sr cm^{-1})$^{-1}$.

where $\sigma(B_i(T_c))$ is the error in the Planck's function at T_c, given as a function of: the surface emissivity error (see section 3.1); the measured surface radiance error obtained after calibration, which was determined to be $\pm 1.9 \times 10^{-5}$ mW $(\text{cm}^2\,\text{sr}\,\text{cm}^{-1})^{-1}$ for CE 312 channel 3 in this case (± 0.13 K in terms of brightness temperature; see section 2); and the error in the hemispheric downwelling sky radiance. This last error can be determined from equation (8) in terms of: the observed cloud cover error, i.e. ± 1 octa; the downwelling sky radiance error for the completely clear sky, $\sigma(L^{\downarrow}_{i\ atm\ hem,NC})$, which has an average value of ± 0.00007 mW $(\text{cm}^2\,\text{sr}\,\text{cm}^{-1})^{-1}$, and corresponds to the mean difference between the simulated values and the direct measurements, since this difference was always larger than the MODTRAN 4 retrieved radiance error of 2% (Thome *et al.* 1998); and the cloud downwelling sky radiance error, $\sigma(L^{\downarrow}_{i\ atm\ hem,C})$, which is calculated from equation (7) using the $\sigma(m_i)$ and $\sigma(n_i)$ values of table 4 and an uncertainty of 2% for H measured by the ceilometer, $\sigma(H)$.

Finally, considering all error sources, an average total T_c uncertainty of ± 0.2 K (with a maximum of 0.3 K and a minimum of 0.16 K) was estimated for the data measured during the campaign.

5. Results

The T_c and T_a measurements obtained were correlated with measurements of PRI, and also PAR, global, direct and diffuse radiation, and wind speed. The PRI is defined as the relative change in reflectance at 531 nm with respect to that at 570 nm (PRI = R531 − R570/R531 + R570) (Gamon *et al.* 1992, Peñuelas *et al.* 1995). This index is linked to xanthophyll-related dynamic changes in non-photochemical quenching (NPQ) of chlorophyll fluorescence, and so it has been shown to be a possible indicator of NPQ (Evain *et al.* 2004).

Figure 3 shows the evolution of T_c and PRI for several clear days, where an inverse correlation between T_c and PRI appears, with a coincidence between T_c

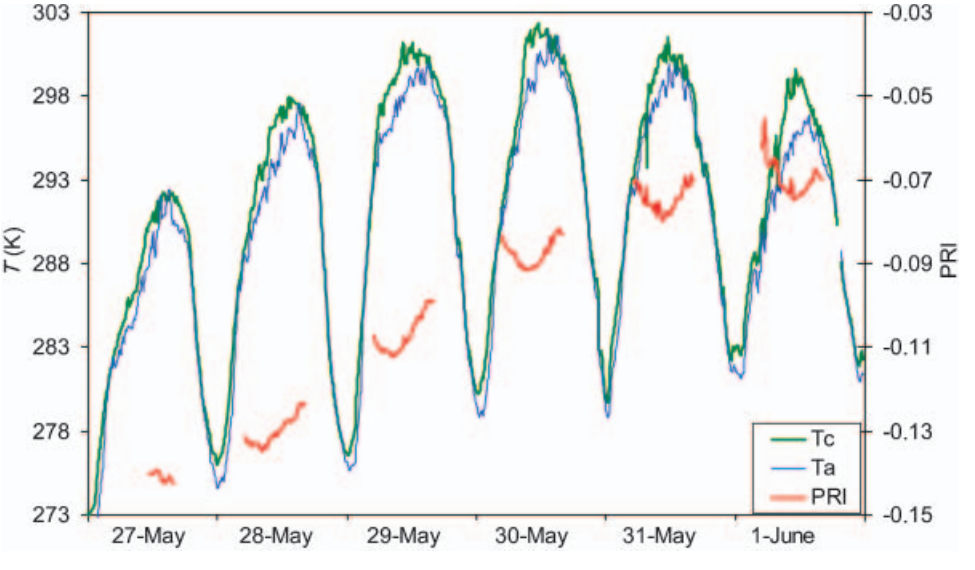

Figure 3. Comparison of PRI, T_c and T_a for several clear days during the campaign (from 27 May to 1 June 2002).

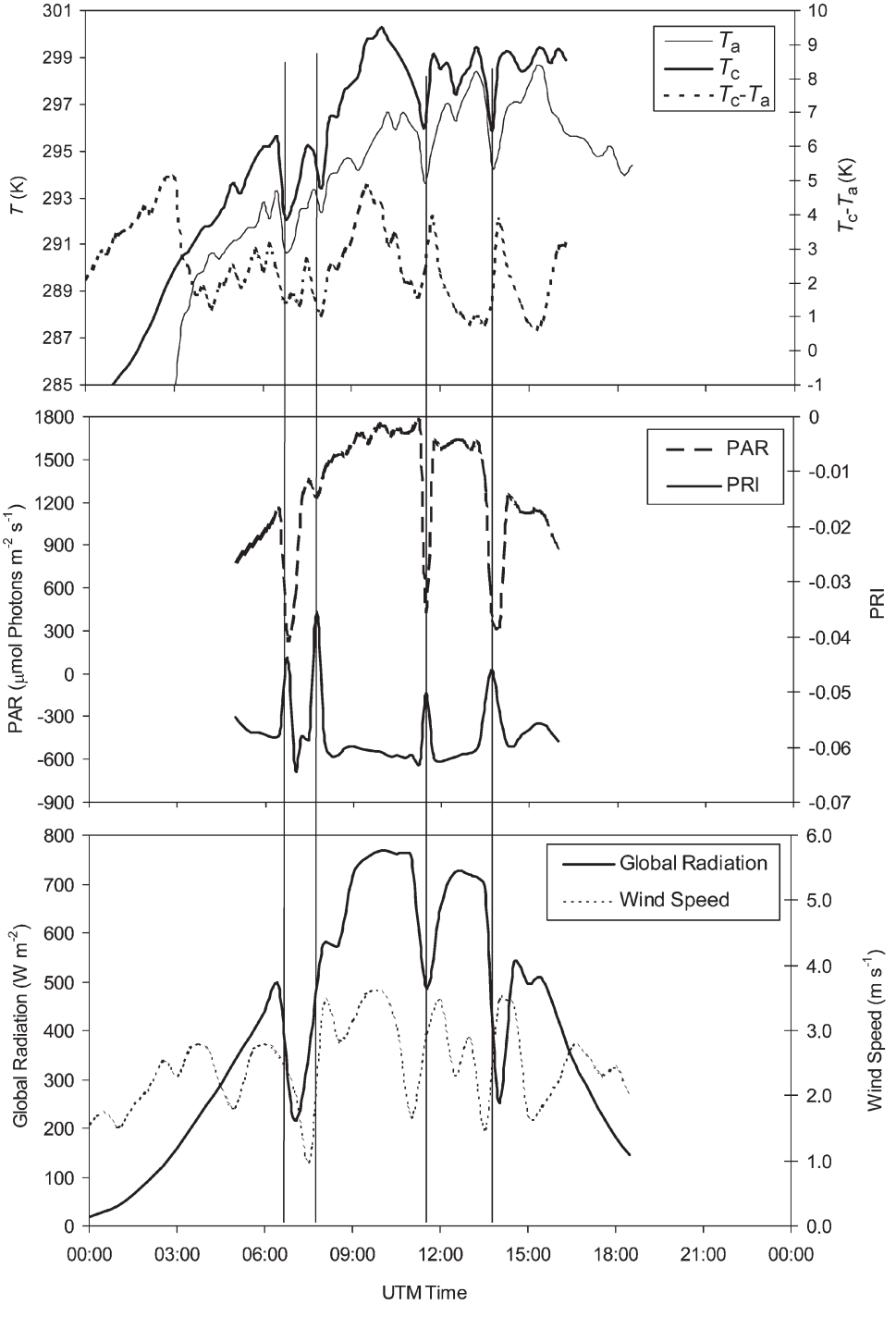

Figure 4. Data comparison for 9 June 2002, showing T_c, T_a and $T_c - T_a$; PAR and PRI; and global radiation and wind speed.

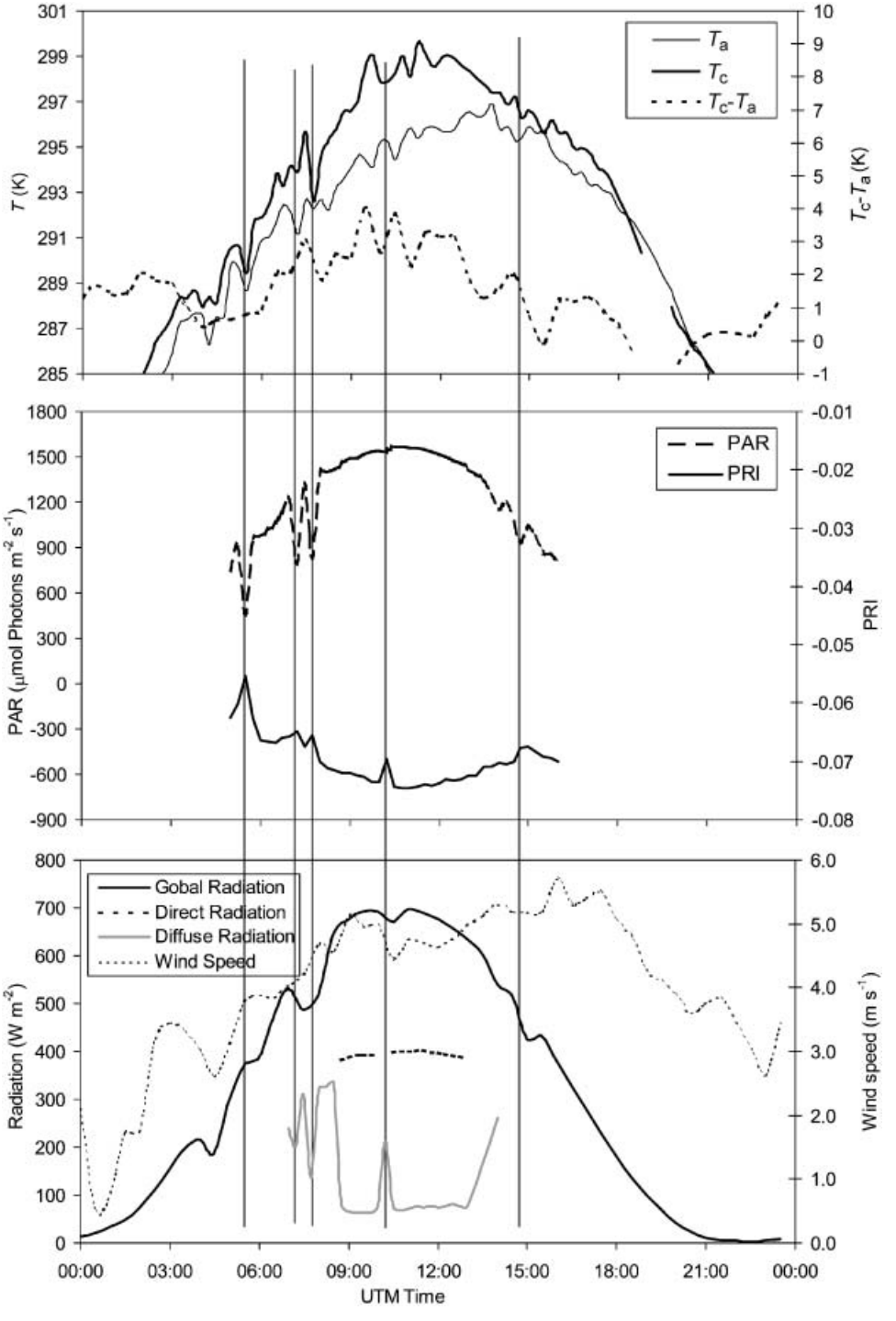

Figure 5. Data comparison for 1 June 2002, showing T_c, T_a and $T_c - T_a$; PAR and PRI; and global, direct and diffuse radiation and wind speed.

maxima and PRI minima. Figure 4 is a detailed analysis of the evolution of these magnitudes for 9 June 2002. Several peaks in the PRI are observed simultaneously to T_c decreases. Additionally, the PRI is inversely correlated with the PAR radiation. Nevertheless, the largest PRI peak coincides with a small PAR change. The direct relationship between T_c and PAR, and the inverse correlation of both with PRI, are observed on more days, e.g. for 1 June 2002 (see figure 5). There are again several PRI peaks correlated inversely with T_c and PAR, but a peak in the PRI simultaneous to a T_c decrease is observed at about 10:05 UTM, not coincident with a PAR decrease. At the same time a wind speed reduction and a peak in the diffuse radiation are apparent, due to a momentary covering of the sun by a cloud, as shown by continuous sky photographs taken in the region. Moreover, the PRI peak seems to be correlated with a reduction in the canopy–air temperature difference, $T_c - T_a$.

6. Summary and conclusions

The purpose of this work was to develop a methodology in order to measure accurate canopy and air temperatures under skies with partial cloud cover, since their changes seem to be related to the variation in PRI, which has been shown to be a possible indicator of NPQ (Evain *et al.* 2004).

A CE 312 radiometer with a channel placed in the spectral region 10.5–11.5 μm (channel 3) was used during the SIFLEX-2002 campaign to autonomously measure canopy radiance, for which the atmospheric correction was considered negligible due to the short atmospheric path between surface and radiometer. However, hemispheric downwelling sky radiance estimates were necessary in order to account for the reflection term in the emissivity correction. This last correction was calculated using emissivity values measured with the box method (Rubio *et al.* 1997, 2003), and the hemispheric downwelling sky radiance was determined considering the sky conditions at the time of measurement.

A new strategy was developed to estimate this sky radiance under partial cloud cover conditions, when the usual approximations are not applicable since they are only suitable for homogeneous skies. This strategy uses cloudiness cover, measured in octas, and cloud base height as input parameters. Using this methodology, canopy temperature was finally determined with an uncertainty of ± 0.2 K during this campaign.

An analysis of temperature changes and PAR and PRI variations shows a relationship between them. An inverse correlation between PRI and canopy temperature, canopy–air temperature difference, solar illumination conditions (mainly PAR radiation) and wind speed was observed from the SIFLEX-2002 data.

The described methodology is not limited to this kind of surface but can be applied to any land surface, either only measuring the target emissivity or using values from existing emissivity databases (Salisbury and D'Aria 1992, Rubio *et al.* 1997, 2003), and having available data on cloudiness amount and cloud height. Cloudiness information can be obtained with a weather station, and allows correction of data for the downwelling sky radiance effect under partial cloud cover conditions; this cloudiness information is not required for completely clear or cloudy skies, when the existing approximations can be used.

Acknowledgement

This work was supported by the European Space Agency through the SIFLEX-2002 project (ESA/ESTEC Contract No. 16026/02/NL/SF), the Spanish Ministerio de

Ciencia y Tecnología by means of Contracts REN2001-3116/CLI and 'Ramon y Cajal' of Dr. E. Valor, the European Union (FEDER funds) and the Generalitat Valenciana (project GV2004-B-084). The Spanish Ministerio de Educación, Cultura y Deportes is acknowledged for the research grant received by Dr. R. Niclòs, and also the University of Valencia for the grant 'V Segles' to J. M. Sánchez and the current contract of Dr R. Niclòs (Ministerio de Educación y Ciencia, CGL2004-06099-C03-01/CLI). The authors also wish to thank the Finnish Meteorological Institute (FMI, Helsinki, Finland) and the Laboratoire pour l'Utilisation du Rayonnement Electromagnétique (LURE, Orsay, France) for their essential contributions during campaign development, and for the weather, PRI and PAR data used in the study.

References

AURELA, M., LAURILA, T. and TUOVINEN, J.P., 2001, Seasonal CO_2 balances of a subarctic mire. *Journal of Geophysical Research*, **106**, pp. 1623–1638.

BALDOCCHI, D.D. and VOGEL, C.A., 1997, Seasonal variation of energy and water vapor exchange rates above and below a boreal jack pine forest canopy. *Journal of Geophysical Research*, **102**, pp. 28939–28951.

BERK, A., ANDERSON, G.P., ACHARYA, P.K., CHETWYND, J.H., BERNSTEIN, L.S., SHETTLE, E.P., MATTHEW, M.W. and ADLER-GOLDEN, S.M., 1999, *MODTRAN 4 User's Manual* (Hascom AFB, MA: Air Force Research Laboratory, Space Vehicles Directorate, Air Force Materiel Command).

BURKE, E.J. and STEWART, J.B., 1997, Test of a sensible heat flux–radiometric surface temperature reationship for Hapex-Sahel. *Boundary Layer Meteorology*, **84**, pp. 329–337.

CACHORRO, V.E., UTRILLAS, M.P., MARTINEZ-LOZANO, J.A. and DE FRUTOS, A.M., 1997, A preliminary assessment of a detailed two stream band model using spectral radiation measurements. *Solar Energy*, **61**, pp. 265–273.

EVAIN, S., CAMENEN, L. and MOYA, I., 2001, Three channels detector for remote sensing of chlorophyll fluorescence and reflectance from vegetation. In *Eighth International Symposium on Physical Measurements and Signatures in Remote Sensing* (Aussois, France: CNES), pp. 395–400.

EVAIN, S., FLEXAS, J. and MOYA, I., 2004, A new instrument for passive remote sensing. 2. Measurement of leaf and canopy reflectance changes at 531 nm and their relationship with photosynthesis and chlorophyll fluorescence. *Remote Sensing of Environment*, **91**, pp. 175–185.

FLEXAS, J., BRIANTAIS, J.M., CEROVIC, Z.G., MEDRANO, H. and MOYA, I., 2000, Steady-state and maximum chlorophyll fluorescence responses to water stress in grapevine leaves: a new remote sensing system. *Remote Sensing of Environment*, **73**, pp. 283–297.

GAMON, J.A., PENUELAS, J. and FIELD, C.B., 1992, A narrow-waveband spectral index that tracks diurnal changes in photosynthetic efficiency. *Remote Sensing of Environment*, **41**, pp. 35–44.

KONDRATYEV, K.Y., 1969, *Radiation in the Atmosphere* (New York: Academic Press).

LEGRAND, M., PIETRAS, C., BROGNIEZ, G., HAEFFELIN, M., ABUHASSAN, N.K. and SICARD, M., 2000, A high-accuracy multiwavelength radiometer for in situ measurements in the thermal infrared. 1. Characterization of the instrument. *Journal of Atmospheric and Oceanic Technology*, **17**, pp. 1203–1214.

LONNQVIST, J., 1995, Experiences with a novel single-lens cloud height lidar. In *Ninth Symposium on Meteorological Observations and Instrumentation* (Boston: American Meteorological Society), pp. 106–109.

MOYA, I., OUNIS, A., LOUIS, J., EVAIN, S. and DUCRUET, J.-M., 2002, Passive fluorescence measurements during SIFLEX. Remote sensing of solar-induced vegetation. In

Proceedings of the FLEX Workshop (Noordwijk, The Netherlands: ESTEC-ESA), R.A. Harris (Ed.). Published on CD-ROM (ESA SP-527), pp. 20.1.

PEÑUELAS, J., FILELLA, I. and GAMON, J.A., 1995, Assessment of photosynthetic radiation-use efficiency with spectral reflectance. *New Phytologist*, **131**, pp. 291–296.

RUBIO, E., CASELLES, V. and BADENAS, C., 1997, Emissivity measurements of several soils and vegetation types in the 8–14 μm wave band: analysis of two field methods. *Remote Sensing of Environment*, **59**, pp. 490–521.

RUBIO, E., CASELLES, V., COLL, C., VALOR, E. and SOSPEDRA, F., 2003, Thermal-infrared emissivities of natural surfaces: improvements on the experimental set-up and new measurements. *International Journal of Remote Sensing*, **24**, pp. 5379–5390.

SALISBURY, J.W. and D'ARIA, D.M., 1992, Emissivity of terrestrial materials in the 8–14 μm atmospheric window. *Remote Sensing of Environment*, **42**, pp. 83–106.

SELLERS, P., HALL, F., MARGOLIS, H., KELLY, B., BALDOCCHI, D., DEN HARTOG, G., CIHLAR, J., RYAN, M.G., GOODISON, B., CRILL, P., RANSON, K.J., LETTENMAIER, D. and WICKLAND, D.E., 1995, The Boreal Ecosystem–Atmosphere Study (BOREAS): an overview and early results from the 1994 field year. *Bulletin of the American Meteorological Society*, **76**, pp. 1549–1577.

THOME, K., PALLUCONI, F., TAKASHIMA, T. and MASUDA, K., 1998, Atmospheric Correction of ASTER. *IEEE Transactions on Geoscience and Remote Sensing*, **36**, pp. 1199–1211.